SLAC–PUB–7664
October 1997

Electron-Cloud Instability and Beam-Induced Multipacting in the LHC and in the VLHC*

F. Zimmermann
Stanford Linear Accelerator Center
Stanford University, Stanford, CA 94309, USA

In the beam pipe of the Large Hadron Collider (LHC), photoemission and secondary emission give rise to a quasi-stationary electron cloud, which is established after a few bunch passages. The response of this electron cloud to a transversely displaced bunch resembles a short-range wakefield and can cause a fast instability. In addition, beam-induced multipacting of the electrons may lead to an enhanced gas desorption and an associated pressure increase. In this paper we report preliminary simulation results of the electron-cloud build-up both in a dipole magnet and in a straight section of the LHC at top energy. The effective wakefield created by the electron cloud translates into an instability rise time of about 40 ms horizontally and 500 ms vertically. This rise time is not much larger than that of the resistive-wall instability at injection energy. Similar simulation studies show that the instability rise time for the proposed Very Large Hadron Collider (VLHC) is about 3–4 s in both transverse planes. The smaller growth rate in the VLHC, as compared with the LHC, is primarily due to the much lower bunch population.

Presented at the International Workshop on Multi-Bunch Instabilities in Future Electron and Positron Accelerators (MBI97), KEK, Tsukuba, Japan, July 15–18, 1997

*Work supported by the U.S. Department of Energy contract DE–AC03–76SF00515, by the European Laboratory for Particle Physics (CERN) and by the Tsukuba EXPO'85 Memorial Foundation.

Electron-Cloud Instability and Beam-Induced Multipacting in the LHC and in the VLHC*

Frank Zimmermann

Stanford Linear Accelerator Center, Stanford University, CA 94309

Abstract

In the beam pipe of the Large Hadron Collider (LHC), photoemission and secondary emission give rise to a quasi-stationary electron cloud, which is established after a few bunch passages. The response of this electron cloud to a transversely displaced bunch resembles a short-range wakefield and can cause a fast instability [1]. In addition, beam-induced multipacting of the electrons may lead to an enhanced gas desorption and an associated pressure increase [2]. In this paper we report preliminary simulation results of the electron-cloud build-up both in a dipole magnet and in a straight section of the LHC at top energy. The effective wakefield created by the electron cloud translates into an instability rise time of about 50 ms horizontally and 400 ms vertically. This rise time is not much larger than that of the resistive-wall instability at injection energy. Similar simulation studies show that the instability rise time for the proposed Very Large Hadron Collider (VLHC) is about 3–4 s in both transverse planes. The smaller growth rate in the VLHC, as compared with the LHC, is primarily due to the much lower bunch population.

1 INTRODUCTION

The LHC is the first hadron storage ring with a significant synchrotron radiation and an accompanying large number of photoelectrons. The total number of photons emitted per turn is comparable to that for the positron ring (LER) of the PEP-II B factory, under construction at SLAC. While in PEP-II an antechamber absorbs ~99% of the photons, this is not the case for the LHC, and, therefore, the total number of photons hitting the beam screen per meter is about 5 times higher.

At a beam energy of 7 TeV, the critical photon energy in a dipole magnet is 44 eV. For this photon energy, the photoemission yield (i.e., the number of photoelectrons emitted per penetrated photon) is close to its maximum value of about 0.1. The emitted photoelectrons are accelerated by the beam field to an energy of a few 100 eV. Since, for most materials, the secondary emission yield for incident electron energies above 100 eV is larger than 1, these photoelectrons generate more secondary electrons, when they again hit the beam screen.

Therefore, an avalanche production of secondary electrons becomes possible, where the electron density increases with every new bunch passing by. Our simulation indicates that the build-up of the electron cloud saturates when the repelling electron space charge on average neutralizes the field of the beam. The stationary electron cloud can be removed by a gap in the bunch train, after which the electron-cloud build-up commences again.

One example of a high-energy proton collider in the post-LHC era is the proposed Very Large Hadron Collider (VLHC), also known as the 'pipetron'. The secondary emission yield of its aluminum vacuum chamber is much higher than that of the LHC copper beam screen, which could increase the charge density and, thus, the effect of the electron cloud. On the other hand, the higher beam energy (increased stiffness of the beam and higher critical photon energy) and the reduced charge per bunch will weaken the instability. A further difference between the two storage rings is the much flatter geometry of the VLHC vacuum chamber. This may change the dynamical response of the electron cloud, since the secondary emission yield depends strongly on the angle of incidence. Parameters for the LHC and the VLHC are listed in Table 1.

storage ring	LHC	VLHC
beam energy E (TeV)	7	50
number of particles / bunch N_b	10^{11}	10^{10}
beam current I (A)	0.54	0.09
hor. r.m.s. beam size σ_x (mm)	0.303	0.089
vert. r.m.s. beam size σ_y (mm)	0.303	0.089
r.m.s. bunch length σ_z (cm)	7.7	4.3
bunch spacing L_{sep} (m)	7.48	5.2
bend length l_b (m)	14.2	250
bend field B (T)	8.4	2
bending radius ρ (km)	2.78	83.3
circumference C (km)	26.66	551
vacuum screen half height h (mm)	18.5	9
vacuum screen half width w (mm)	23	20
critical photon energy (eV)	44	500
hor./vert. tune Q	63	247
chamber/beam-screen material	Cu*	Al
chamber/beam-screen temperature	4 K	300 K

Table 1: Parameters of the LHC [3] and the low-field VLHC [4]; *possibly with TiN or TiZr coating [5, 6].

Transverse multi-bunch instabilities attributed to photoelectrons interacting with a train of positron bunches

*Work supported by the US Department of Energy under Contract DE-AC03-76SF00515, by the European Laboratory for Particle Physics (CERN) and by the Tsukuba EXPO '85 Memorial Foundation.

have recently been reported from the KEK photon factory [1, 7] and from BEPC at IHEP in Bejing [8]. An instability of this kind, with a millisecond rise time, is also predicted for the Low Energy Ring of the PEP-II B factory [9, 10, 11]. The electron-cloud instability, sometimes called the 'Ohmi effect' [1], was experimentally observed to occur for short bunch spacings [7], where the photoelectrons cross the beam pipe within a few bunch passages.

Conversely, it has been known since the mid-70s from beam tests with an Al chamber prototype in the ISR [2] that, in the opposite regime of larger bunch spacings, beam-induced multipacting is possible. Here, electrons bounce from wall to wall in resonance with the discrete bunch structure, and, if the secondary emission yield is larger than unity, the number of electrons amplifies exponentially. Increased gas desorption and a local pressure bump were the observable harmful effect [2]. The LHC parameters, listed in Table 1, allow for multipacting, above an approximate threshold of 160 mA total beam current [12], a factor 3 below the design value. In the VLHC, multipacting sets on roughly at the design current. Although they occur for different values of the bunch spacing, electron-cloud instability and multipacting are both caused by the same physical processes and no clear distinction is possible. The LHC and VLHC parameters lie on the border line where either effect can be important.

It may be worthwhile to mention that in the ISR also an electron-driven instability of a coasting proton beam has been observed [13, 14]. The most important differences between the LHC and the ISR are: 1) the LHC beam is bunched and 2) the enormous number of primary photoelectrons in the LHC.

Preliminary simulation results and analytical estimates of the electron-cloud instability in the LHC and the VLHC were presented previously [15, 16, 17]. The LHC instability-growth rates calculated in this paper are about a factor of two to three smaller than those reported in [15], the difference being due to some modifications and corrections of the simulation code (particularly, the calculation of the electron space-charge field and the angular distribution of the secondary electrons were modified) [1].

2 PHYSICS MODEL AND SOME NUMBERS

The number of photons emitted by a charged particle per radian is [18]

$$N_\gamma = \frac{5}{2\sqrt{3}}\,\alpha\,\gamma \qquad (1)$$

where α is the fine-structure constant and γ the Lorentz factor. In the LHC at 7 TeV, this amounts to about 3.7×10^{10} photons per 14.2-m long bend and per proton bunch. For comparison, assuming 1 nTorr hydrogen gas at 10 K, about 3×10^4 electrons per bend and per bunch are generated by ionization of the residual gas. This number is more than 6 orders of magnitude smaller than the number of photoelectrons, which illustrates the significance of the synchrotron radiation in the LHC!

A typical photoemission yield at energies of 10–100 eV is 0.1, see, e.g., Ref. [19]. According to Ref. [20], the reflectivity of the beam pipe material for these photon wavelengths is close to 90%. Thus, one might assume [21] that on average every photon that hits the beam screen is either reflected or converts into a photoelectron, so that the final total number of photoelectrons is approximately equal to the number of radiated photons, or that the 'effective photoemission probability' η_{pe}^{eff} is equal to 1. This is the assumption made in our simulation. Under this assumption, every photon is reflected up to 10 times before it creates a photoelectron, and the impact location on the beam screen can be considered random. For this reason, we launch the photoelectrons uniformly distributed around the beam-screen aperture (idealized as elliptic), with an initial uniform energy distribution between 0 and 10 eV.

It has been conjectured by M. Zisman [22] that the reflectivity of a real beam pipe can be much lower, perhaps as low as 5–10%, in which case we would overestimate the emitted photoelectrons by almost an order of magnitude. We have, therefore, evaluated the sensitivity of the final electron density to the photoemission yield. In many cases, after an initial transient, the build-up and maintenance of the electron cloud is largely determined by the secondary emission, whereas the dependence on the photoemission parameters is not too critical (a similar result was obtained in simulations of the electron-cloud instability for PEP-II [21]).

Photoelectrons emitted from the wall are accelerated by the field of the beam. A photoelectron generated by synchrotron radiation that was emitted from the bunch head acquires the maximum transverse momentum:

$$\Delta p_{el} \approx \frac{2N_b r_e c m_{el}}{r_{pipe}} \qquad (2)$$

where r_e denotes the classical electron radius, c the speed of light, r_{pipe} the radius of the beam pipe, m_{el} the electron mass and p_{el} the electron momentum. For the LHC parameters, $\Delta p_{el}/m_{el} \approx 0.028\ c$, corresponding to an energy of

$$\Delta E_{el} \approx \frac{1}{2} m_{el} c^2 \left(\frac{v}{c}\right)^2 \approx 200\ \text{eV} \qquad (3)$$

and to a wall-to-wall time of flight of about 1.5 m/c. Photoelectrons created by radiation from later parts of the bunch only receive a fraction of the 200-eV maximum energy, and their wall-to-wall time of flight is accordingly larger. Since the bunch spacing is 7.5 m, most of the primary photoelectrons hit the wall, before the next bunch arrives. When an electron of energy ~200 eV impinges on the wall, secondary electrons are emitted. The velocity of these secondary electrons is a factor 5–10 lower than that of the incident electron. These secondary electrons are accelerated, along with the newly generated photoelectrons, when the next bunch passes by. Thus, without an electron space-charge force, the number of electrons would increase indefinitely.

[1] These corrections were suggested by Dr. O. Brüning at CERN.

Most of the LHC circumference is occupied by high-field dipole magnets in which the electron motion is effectively constrained to the vertical direction. The electron cloud in the dipoles is believed to be the dominant 'wakefield' source. Nevertheless, straight sections account for about 20% of the LHC circumference and the electron dynamics is different enough to motivate a separate consideration.

In a vertical magnetic field B of 8.4 Tesla, a 200-eV electron rotates on a circle in the x-z plane with a Larmor radius of about

$$\rho_{el} \approx \frac{p_{el}}{eB} \approx 6\ \mu\mathrm{m} \tag{4}$$

During a bunch passage the horizontal kick is averaged over ~100 cyclotron rotations, with a very small net momentum transfer [23]. Therefore, in the dipole magnets we only apply a vertical kick from the beam. By contrast, in a straight section, the electron receives both a horizontal and a vertical kick from each passing bunch.

The potential at the beam center is given by

$$U \approx \frac{\lambda}{2\pi\epsilon_0} \ln \frac{r_{pipe}}{\sqrt{2}\sigma_y} = \frac{Z_0 I}{2\pi} \ln \frac{r_{pipe}}{\sqrt{2}\sigma_y} \tag{5}$$

where λ denotes the charge line density, Z_0 (=377 Ω) the vacuum impedance, and I the beam current. The average potential is about 120 V, the peak potential (due to bunching) is about 4.2 kV. This number may serve as an estimate for the maximum energy an electron close to the center of the beam pipe might receive in the bunch field.

Many aspects of secondary emission have been discussed in the literature, e.g., in Ref. [24]. In our simulation we have implemented the universal yield curve discussed by Seiler [25], where the secondary emission yield is characterized by two parameters: the primary energy at which the yield is maximum (E_p^m, assumed to be 400 eV) and the maximum yield (the emitted charge per primary charge) for perpendicular incidence, δ_{max}. We have varied δ_{max} between 1.1 (for TiN coated surfaces) and 1.8 (for OFHC copper). The analytical expression for the yield is [25, 26]

$$\delta(E_r,\theta) \approx \delta_{max}\ 1.11\ (E_r)^{-0.35}\ (1 - e^{-2.3\ E_r^{1.35}})/\cos\theta \tag{6}$$

with θ denoting the angle of incidence with respect to the surface normal and $E_r \equiv E_p/E_p^m$, where E_p is the energy of the incident electron. Figure 1 shows the yield δ, Eq. (6), as a function of energy, for two different values of the angle θ. To avoid unphysically large yields, we limit the $1/\cos\theta$ factor to a maximum value of 5. This cut-off is fairly arbitrary at this moment, and could be improved by measurements of the angular-dependent emission yield on beam-screen prototypes.

The energy of the emitted secondary electrons is taken to be uniformly distributed between 1 eV and (in most cases) 20 eV [2]. The initial velocity direction of the secondary electrons is assumed to follow a $\cos\theta$ distribution, with preferred emission in the normal direction [25]. The above assumptions will have to be revised, if a 9-T magnetic field is shown to have a strong effect on the secondary emission yield and on the emission direction.

[2] We can vary the upper energy limit in order to study the effect of the secondary-electron energy distribution on the electron-cloud build-up and on the effective wakefield which it produces.

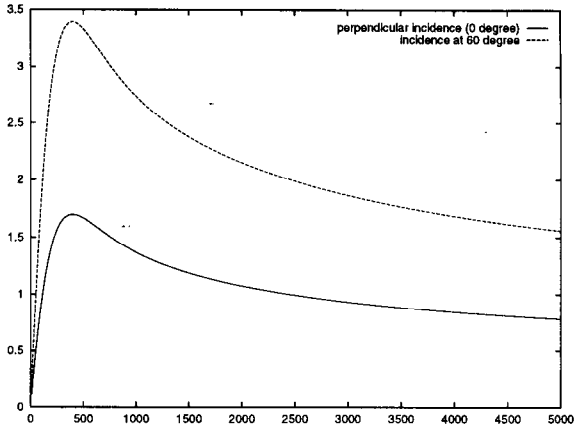

Figure 1: Secondary emission yield, Eq. (6), as a function of the primary electron energy (in eV), for 0° and 60° incident angle with respect to the surface normal; the maximum emission yield for perpendicular incidence was chosen as $\delta_{max} = 1.7$.

We consider each proton bunch as a uniform longitudinal charge distribution of total length $2\sqrt{2}\,\sigma_z$. The bunches are assumed to pass at the center of the beam pipe and are given a constant round cross section. Ignoring the distortion of the beam field due to the slight asymmetry between the horizontal and vertical beam-screen dimensions [27], we calculate the kick on the electrons from a passing bunch using the round-beam formula for free space

$$\Delta\vec{p}_{el} = -\frac{2N_b r_e \vec{r} m_{el} c}{r^2}\left(1 - \exp\left(-\frac{r^2}{2\sigma^2}\right)\right) \tag{7}$$

where $\vec{r}$ is the position of the electron with respect to the center of the beam pipe, $r = |\vec{r}|$, and $\sigma = \sigma_x = \sigma_y$.

We represent the 4×10^{10} photoelectrons generated per bunch and per bend by a set of macroparticles of variable number. Typically we generate 1000 macro-photoelectrons for each bunch, which we distribute over the bend length of 14.2 m. The macroparticle charge of about 4×10^7 e is chosen such that the total photoelectron charge is equal to the real one.

We split each bunch into several slices. After each slice we launch new photoelectrons and apply a kick from the beam. To precisely model the motion of those electrons which are very close the beam the minimum number of slices should be chosen larger than [28]

$$n_{\mathrm{slice}} \approx \frac{8\sqrt{N_b r_e \sigma_z}}{\sigma_x} \tag{8}$$

where N_b denotes the bunch population, r_e the classical electron radius, σ_z the rms bunch length and σ_x ($= \sigma_y$) the

rms transverse beam size. Inserting the LHC parameters into Eq. (8), we find $n_{\rm slice} \approx 130$. To keep the computation time within acceptable bounds, in most simulations we had to choose a much smaller number of slices, $n_{\rm slice} = 5$. As we shall see, in the LHC the main response of the electron cloud comes from electrons whose distance from the beam is at least 20 σ_x. Since this is approximately equal to the critical radius [28],

$$r_C \approx 3\sqrt{N_b r_e \sigma_z/\pi} \tag{9}$$

beyond which a single-slice kick approximation is applicable, we believe that 5 slices per bunch, as used in our simulation, should still assure a reasonable accuracy. The error thus introduced can be estimated by comparing, for a test case, the simulation result using 5 slices with that obtained for a larger number of slices. To some extent, the error induced by the finite number of slices can also be inferred from the variation of the results over different random seeds. We will see that either method gives an error estimate of the order of 10% or less. In much the same manner as the bunches, also the gap between two bunches is divided into a number of steps (typically 7–20). At each step the motion of all macroelectrons is calculated.

When an electron hits the beam screen, we launch one or more secondary electrons at the point of impact, with charge, energy and velocity calculated as described above. The total charge of the emitted secondaries depends on the energy and on the incident angle of the lost electron. In the simulation, the number of re-emitted secondary macroelectrons is always chosen high enough that their charge is less or equal to, but never larger than that of the primary photoelectron [29]. This prevents the undesirable situation that most of the electron charge is carried by very few macroparticles.

In order to limit the growth of the electron cloud, which otherwise would continue indefinitely, the electric space-charge field of the electrons is included in the simulation as well. So far, in most simulations we have treated this field in a very rough approximation, where we assume a radial symmetry and introduce a radial grid of 500 equally spaced circles. Counting the number of electron macroparticles in the different circles, we calculate the electric field at each radial grid point using Gauss' law. Between two grid points we interpolate the field linearly. As for the beam kick, in a dipole magnet the space-charge kick is applied only in the vertical direction, because of the high cyclotron frequency.

Calculating the space-charge force in the way described, we implicitly assume a radial symmetry. As we shall see, this is not always a good approximation. A more accurate simulation would use a two-dimensional FFT of the electron distribution [30] or by a two- (three-) dimensional particle-in-cell simulation [3]. We also note that typically we calculate the electron space-charge field only once in each gap between bunches, and that a more frequent reevaluation, though prohibitively time consuming, might change the simulation results [31].

We believe though that our approximate treatment is adequate to obtain a first estimate of the equilibrium density and of the instability rise time.

In our simulations, the inclusion of the space charge leads to a saturation of the electron-cloud density at a value close to the neutralization level, which we define by the number of photoelectrons that is equal to the time-averaged number of protons.

After a series of bunches have passed, we displace one bunch vertically or horizontally by a certain offset Δy or Δx, and calculate the kick that the disturbed electron cloud exerts on the following bunch. More specifically, for both dipoles and straight sections, we calculate an effective short-range dipole wake function $W_1 \equiv W_1(L_{sep})$ at a distance equal to the bunch spacing L_{sep}, integrated over the circumference, by summing the kicks on the bunch from all the macroelectrons:

$$W_{1,y} = \sum_i \frac{2 y_i Q_i}{N_b r_i^2\ (\Delta y)} \left(1 - \exp\left(-\frac{r_i^2}{2\sigma^2}\right)\right) \frac{C}{l_b} \tag{10}$$

where C denotes the ring circumference, l_b the length of a bending magnet, Q_i the charge of the ith macroelectron, y_i (x_i) its vertical (horizontal) coordinate and r_i the radial distance from the center ($r_i \equiv \sqrt{x_i^2 + y_i^2}$). An equivalent expression is used for the horizontal plane. Due to the peculiar nature of the electron cloud, this wake-function definition could depend on the magnitude of the offset Δy (or Δx) chosen.

To obtain the integrated wake function of the LHC, we take a weighted average over the two different regions considered, i.e.,

$$W_{1,y\ (x)}^{LHC} \approx 0.8 \times W_{1,y\ (x)}^{bend} + 0.2 \times W_{1,y\ (x)}^{straight} \tag{11}$$

where the factors 0.8 and 0.2 are the relative fractions of the LHC circumference that are covered by bending magnets and straight sections, respectively.

From the effective wake functions $W_{1,y}$ and $W_{1,y}$ the instability rise times can be computed. For a first estimate, we consider a train of $M = 3564$ proton bunches (equal to the maximum number of bunch places) uniformly distributed around the ring. Assuming that the wakefield decays rapidly and only affects the next bunch, the complex multibunch betatron frequency shift is [1, 32]:

$$\Omega_{y\ (x)}^{(\mu)} - \omega_{\beta,y\ (x)} = \frac{N_b r_p c^2}{2\gamma C \omega_\beta} W_{1,y\ (x)}\ e^{i2\pi(\mu + Q_{y\ (x)})/M} \tag{12}$$

for $\mu = 0, ..., M-1$, where $Q_{y\ (x)}$ is the vertical (horizontal) betatron tune. The imaginary part of Ω^μ is the instability growth rate of the μth multibunch mode. The instability spectrum is very broadband and covers many modes. The shortest rise times of the fastest growing modes are of the order

$$\tau_{y\ (x)} \approx \frac{4\pi\gamma Q_{y\ (x)}}{N_b r_p c W_{1,y\ (x)}} \tag{13}$$

[3] Recently, O. Brüning from CERN has written a refined routine, which calculates the space-charge field on a 2-dimensional grid.

where $Q_{y\,(x)}$ ($= C\omega_{\beta,y\,(x)}/(2\pi c)$) is the vertical (horizontal) betatron tune. If there are clearing gaps and the ring is not uniformly filled, the (vertical) amplitude of the nth consecutive bunch increases as

$$y_n \sim \frac{1}{n!}\left(\frac{N_b r_p c W_{1,y} t}{4\pi\gamma Q_y}\right)^n \hat{y}_0 \qquad (14)$$

where t is the time and $\hat{y}_0$ an initial perturbation of the first bunch in the train. For large values of n, Eq. (14) approaches an exponential behavior with a time constant identical to that in Eq. (13).

3 SIMULATION RESULTS FOR THE LHC

Figure 2 presents a typical electron-charge build-up inside an LHC bending magnet. The charge increase as a function of time is shown for two different secondary-emission yields. As can be seen, in both cases the charge density saturates after the passage of less than 10 bunches. The neutralization density for these parameters corresponds to a total electron charge of about 2×10^{11} e, which is not far from the saturation values observed in Fig. 2. Figure 3 (top) compares the unlimited charge increase without space charge with the saturated behavior that is observed when the electron space charge is included. The repelling space-charge field is calculated using the radially symmetric approximation outlined above. An example is shown in Fig. 4. The space-charge field increases roughly linearly with the radius, which would be consistent with a fairly uniform electron distribution.

Almost all the results discussed in this report were obtained assuming a photon reflectivity of 90%. If the real reflectivity is lower, less photoelectrons will be emitted. Figure 3 (bottom) shows how, in the simulation, the electron cloud builds up more slowly, when the number of photoelectrons is reduced.

In Fig. 5, the transverse macroparticle distribution after 40 bunches is depicted for two different values of the secondary-emission yield δ_{max}. For small values of δ_{max} (top figure), the electron density is fairly uniform, which is consistent with the linear increase of the electric space-charge field in Fig. 4. For large values of δ_{max} (bottom figure), two broad vertical stripes of increased electron density emerge. The path of a macroelectron and of all its descendants is constrained by the magnetic field to the same horizontal position, which leads to the appearance of many narrow vertical lines compounding these two stripes. The two vertical stripes are located at a horizontal distance of about $\pm 20\ \sigma$ (6 mm) from the beam-pipe center.

Figure 6 shows that at this horizontal position the maximum electron energy after the passage of a bunch is about equal to the characteristic energy E_p^m for which the secondary-emission yield is maximum (see Fig. 1). In Figure 6, we also demonstrate the effect of different choices for the number of tracking steps per bunch passage. The typically chosen 5 tracking steps per bunch (bottom picture) give an unphysically large value for the maximum energy of electrons close to the center of the beam pipe, as

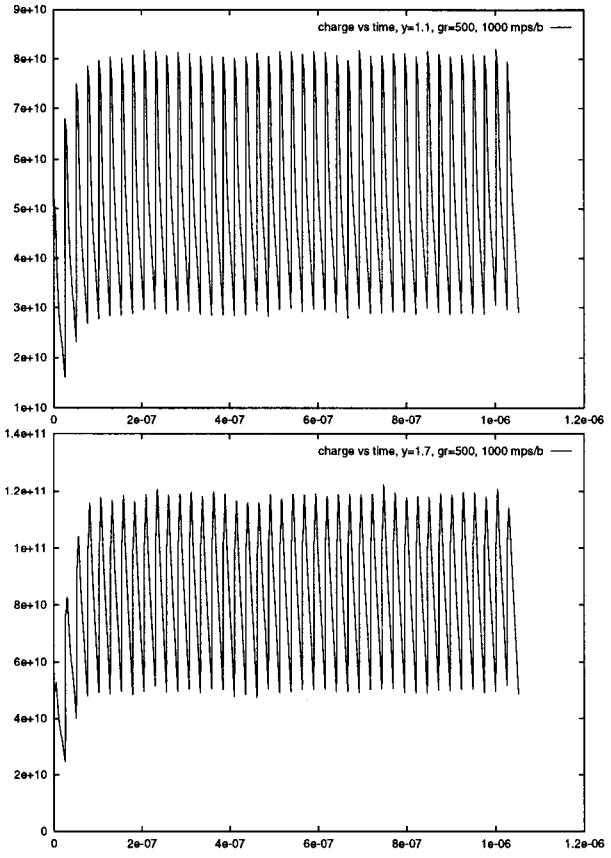

Figure 2: Charge of the electron cloud (in units of e) accumulated inside an LHC bending magnet as a function of time (in s), for two different values of the maximum yield δ_{max}; top: $\delta_{max} = 1.1$; bottom: $\delta_{max} = 1.7$. The total time span corresponds to 41 bunch passages, which are reflected in the sawtooth-like evolution pattern. In this simulation, 1000 macroparticles per bunch were launched, and the grid size was 500 points.

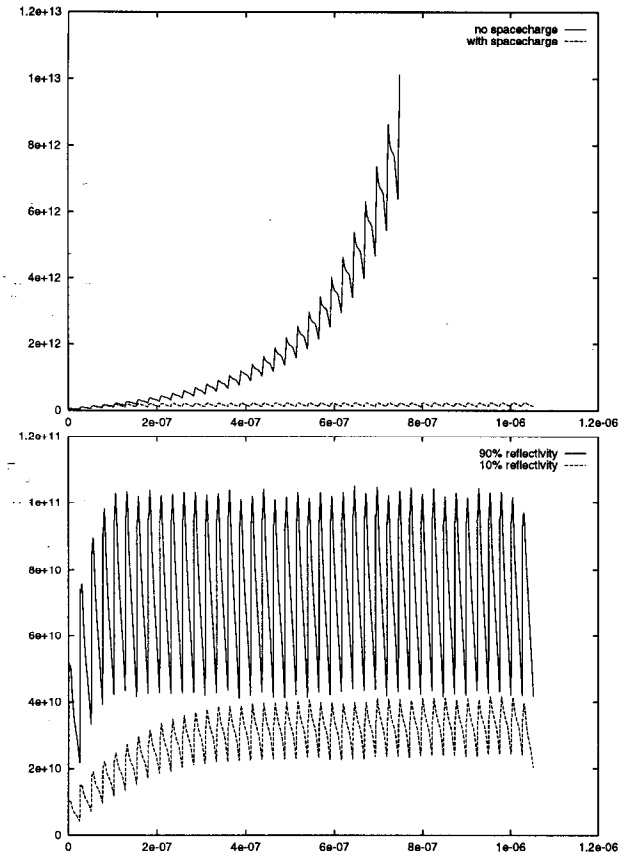

Figure 3: Charge of the electron cloud (in units of e) accumulated in an LHC bending magnet as a function of time (in s); top: with and without space charge; bottom: with an emission probability η_{pe}^{eff} of 1 photoelectron/photon (corresponding to 90% photon reflectivity at the beam screen) and with an effective emission probability of only 0.2 photoelectrons per photon (corresponding to a reduced photon reflectivity). A maximum secondary-emission yield δ_{max} of 1.5 was assumed.

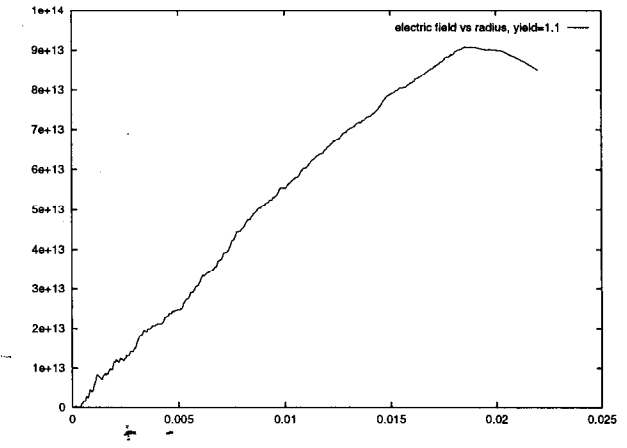

Figure 4: Electron acceleration (in m/s^2) due to the electric self-field of the electron cloud in an LHC bending magnet as a function of radius (in m), after 40 bunches; a maximum secondary-emission yield of $\delta_{max} = 1.1$ was assumed.

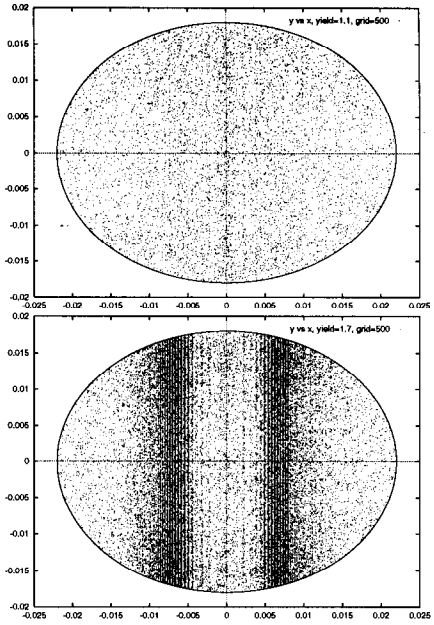

Figure 5: Transverse distribution of macroelectrons in an LHC bending magnet after 40 bunches for a maximum secondary emission yield δ_{max} of 1.1 (top) and 1.7 (bottom). Horizontal and vertical dimensions are given in units of m.

was already speculated in Ref. [28]. For the larger number of 50 steps per bunch (top picture), the maximum energy is close to the correct value calculated in [28]. Figure 7 demonstrates that the high-density region moves towards the center, when the beam current is decreased, as one might have expected.

Projected horizontal and vertical electron charge distributions are displayed in Figs. 8 and 9. Comparison of the top and bottom figures shows that the observed large fluctuations in the simulation results are of statistical nature, due to the finite number of macroparticles, and that they can be reduced by averaging over several random seeds. Figure 10 illustrates the perturbation of the horizontal charge distribution which is induced by a horizontally displaced bunch. It is this perturbed distribution that causes the wakefield effect.

A typical variation of the deduced wake functions for different random seeds is depicted in Fig. 11. In order to obtain reliable estimates of the dipole wake function W_1, we usually performed simulations for 10 different random seeds. For each random seed, we computed the average of the kicks for a positive and a negative offset—correcting for the relative sign of kick and offset—, to further reduce the statistical fluctuation of the result.

Simulation results for a variety of conditions are summarized in Table 2. The horizontal wakefield in the bending magnets is found to be the predominant effect. A probable reason for this is the increased and nonuniform charge density in the horizontal plane (see Figs. 8 and 10).

The computed wake functions are fairly indepen-

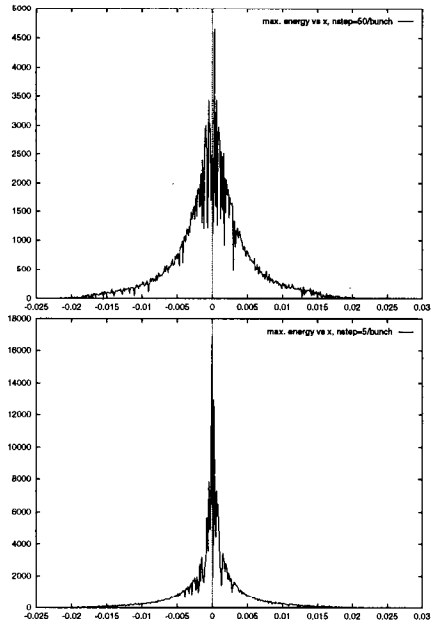

Figure 6: Maximum energy (in eV) of photoelectrons and secondary electrons in an LHC bending magnet after the passage of the 41st bunch as a function of the horizontal electron position (in m), obtained by simulations using 50 tracking steps per bunch passage (top) and 5 tracking steps per bunch passage (bottom). In both pictures electron energies for which the secondary-emission yield is maximum (~400 eV) are found about 5–8 mm from the beam-pipe center. The enhanced secondary emission in this region could explain the strong nonuniformity of the horizontal distribution seen in the bottom part of Fig. 5.

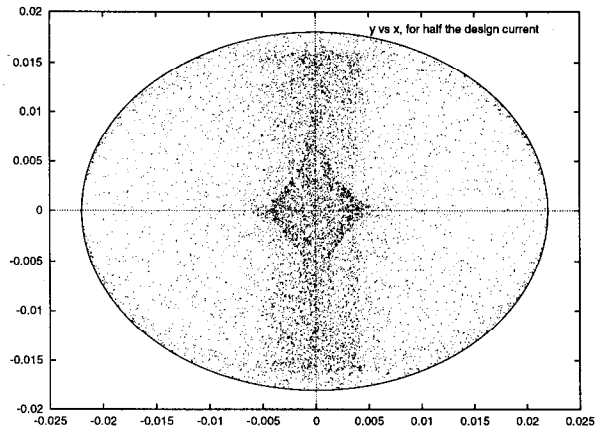

Figure 7: Transverse distribution of macroelectrons in an LHC bending magnet after 40 bunches with half the design current per bunch. The maximum secondary emission yield δ_{max} is 1.7. Horizontal and vertical dimensions are given in units of m.

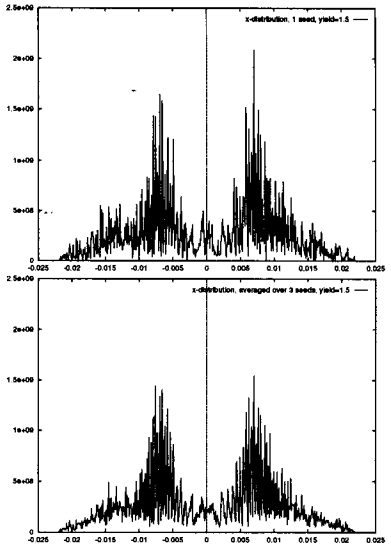

Figure 8: Projected horizontal electron charge density in an LHC bending magnet after 40 bunches, as obtained for one random seed (top) and averaged over three different seeds (bottom). The horizontal coordinate is given in units of meters; the vertical coordinate is the charge (in units of e) per bending magnet, per bin and per grid point. The total number of grid points is 500. The maximum yield is $\delta_{max} = 1.5$, and 1000 macroparticles per bunch (and per seed) were used.

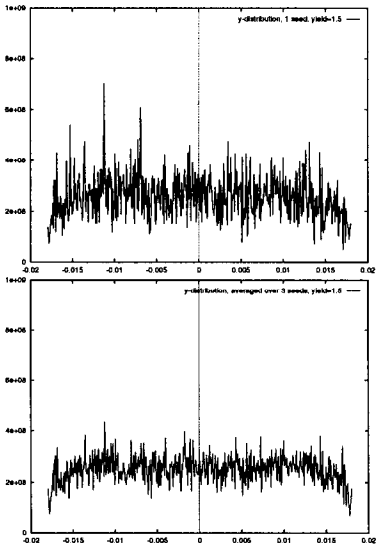

Figure 9: Projected vertical electron charge density in an LHC bending magnet after 40 bunches, as obtained for one random seed (top) and averaged over three different seeds (bottom). The horizontal coordinate is given in units of meters; the vertical coordinate is the charge (in units of e) per bending magnet, per bin and per grid point. The total number of grid points is 500. The maximum yield was chosen as $\delta_{max} = 1.5$, and 1000 macroparticles per bunch (and per seed) were used.

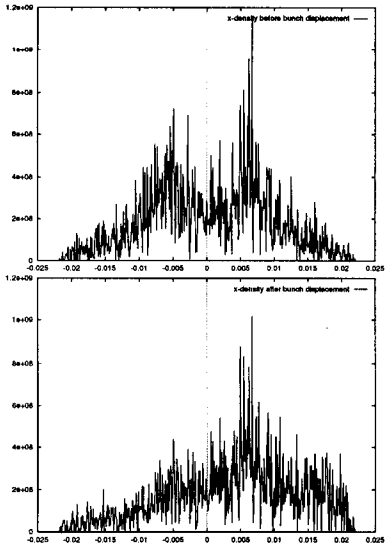

Figure 10: Projected horizontal electron charge density in an LHC bending magnet after about 40 bunches; top: before the 41st bunch is horizontally displaced by 1 cm; bottom: just prior to the arrival of the 42nd bunch. The horizontal axis is in units of meters; the vertical coordinate is the charge (in units of e) per bin and per grid point. The total number of grid points is 500. The maximum yield was chosen as $\delta_{max} = 1.7$, and 1000 macroparticles per bunch were used.

dent of the bunch offset Δy (Δx) chosen, but the statistical error increases when the displacement is reduced. Simulations performed with varying numbers of macroparticles give almost identical results. Similarily, increasing the number of tracking steps for the gap between bunches only has a small impact on the result.

Lowering the maximum secondary-emission yield from 1.5 to 1.1 reduces the wakefield by less than a factor of 2. The moderate dependence of the wakefield on the secondary-emission yield and the secondary-electron energy suggests that the wakefield is not fully determined by the secondary emission, but that the photon reflectivity, the photoemission yield and the initial photoelectron distribution also have a significant influence on the computed wakefield.

If the beam current is a factor 2 smaller than the design value (*i.e.*, $N_b \approx 5 \times 10^{10}$) the effective horizontal wakefield increases by about 25%! The wakefield does not decrease in proportion to the beam current, because, for lower current, the high-density region of the electron cloud is closer to the beam-pipe center (Fig. 7). This aspect will be important for the design specification of a multibunch feedback system.

Reducing the number of photoelectrons emitted per photon by a factor of 5 results in a 25% smaller wakefield (in Table 2 this case is indicated by the comment '$\eta_{pe}^{eff} = 0.2$').

Since the gap between bunch passages is much

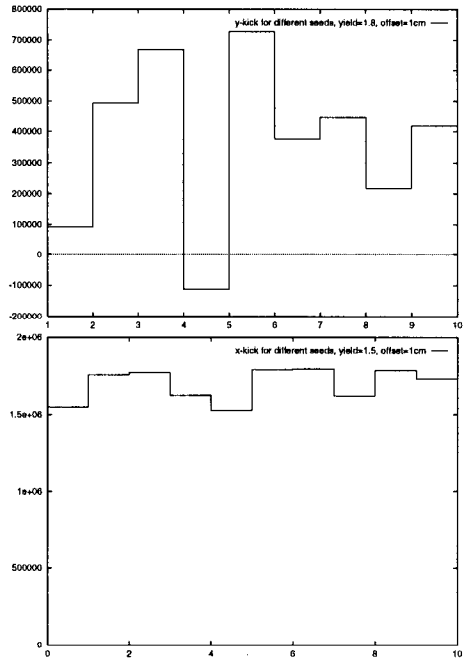

Figure 11: Vertical and horizontal wake function $W_1(L_{sep})$ for an LHC bending magnet in units of m^{-2} as computed with 10 different random seeds. In these simulations, we assumed a maximum secondary-emission yield of $\delta_{max} = 1.8$ (top) and $\delta_{max} = 1.5$ (bottom). The vertical (horizontal) offset was Δy (Δx) = 1 cm, and 1000 (3000) macro-photoelectrons were launched per bunch. (Note that the average wake is $\sim 20\%$ larger than that listed in Table 2. This is due to both the smaller number of interbunch tracking steps (7 compared with 20 used for Table 2), and also the larger yield value $\delta_{max} = 1.8$ in the upper histogram.)

longer than the average travel time of the primary photoelectrons, the majority of electrons which are still present when the next bunch passes by are low-energetic secondary electrons. (Fast secondary electrons also get lost in the interbunch gap.) Therefore, one may suspect that the effective wakefield depends strongly on the secondary-electron energy distribution [33]. To study this dependence we have performed a series of simulations where the energy of the emitted secondary electrons was uniformly distributed between 1 eV and a variable maximum value E_{max}. When we decrease the maximum energy from 20 eV to 5 eV, the horizontal (vertical) wakefield decreases (increases) by about 25% (170%!). In Table 2 this case is indicated by the comment '$E_{max} = 5$ eV'. Simulation results for different E_{max} values are summarized in Fig. 12, which confirms that, while the horizontal wake is fairly independent of the parameter E_{max}, the vertical wake function is strongly affected by it. The latter changes its sign at a certain value of E_{max} for which about half of the secondary electrons cross the center of the vacuum chamber prior to the arrival of the following bunch.

Finally, increasing the number of slices per bunch from 5 to 20 or 50 changes the simulated horizontal wakefield by less than 5%.

δ_{max}	$W_{1,y}$ (10^5m^{-2})	$W_{1,x}$ (10^6m^{-2})	comment
1.5	3.0 ± 2.5	2.8 ± 0.2	—
1.5	5.6 ± 0.2	2.2 ± 0.04	3000 mps./b.
1.5	4.5 ± 3.6	2.3 ± 0.6	$\Delta x, y = 5$ mm
1.5	not calc.	3.5 ± 0.4	$N_b = N_{b0}/2$
1.5	not calc.	2.1 ± 0.1	$\eta_{pe}^{eff} = 0.2$
1.1	0.2 ± 0.07	1.7 ± 0.1	—
1.7	2.2 ± 1.3	3.1 ± 0.2	—
1.5	1.0 ± 1.0	0.22 ± 0.15	drift
1.5	8.2 ± 1.0	2.1 ± 0.1	$E_{max} = 5$ eV
1.5	not calc.	2.7 ± 0.20	$n_{\rm slice} = 20$
1.5	not calc.	2.7 ± 0.25	$n_{\rm slice} = 50$

Table 2: Effective LHC bunch-to-bunch dipole wake function extracted from the simulation, for various secondary emission yields, macroparticle numbers, transverse offsets, charges per bunch, and effective photoemission yields. All simulations were performed using 1000 macroparticles per bunch (mps/b.) and with a transverse drive-bunch displacement Δx (Δy) equal to 1 cm, unless commented otherwise. In all cases, the effective wake function in a bending magnet is quoted, except for one row, which considers a drift space. The comments $\eta_{pe}^{eff} = 0.2$ and $N_b = N_{b0}/2$ refer to a reduction of the photoemission probability and of the beam current by a factor of 5 or 2, respectively, compared with the nominal case. In the case denoted '$E_{max} = 5$ eV' the maximum energy of the secondary electrons was reduced from 20 eV to 5 eV. The last two rows represent simulations where the number of slices per bunch was raised to 20 and 50, respectively (in all other cases this number was 5).

From Table 2, the integrated dipole wake functions

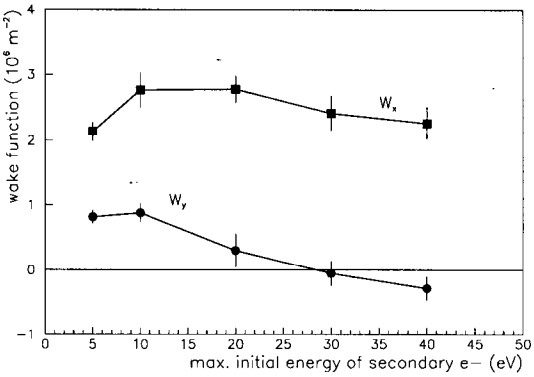

Figure 12: Vertical and horizontal wake function for an LHC bending magnet as a function of the maximum secondary-electron energy E_{max}, assuming a uniform energy distribution between 1 eV and E_{max}. In these simulations, the yield parameters was chosen as $\delta_{max} = 1.5$, and 1000 macroparticles per bunch were used.

$W_{1,x}^{LHC}(L_{sep})$ and $W_{1,y}^{LHC}(L_{sep})$ of Eq. (11) are about 2.5×10^6 m^{-2} and 3.0×10^5 m^{-2}, respectively, for the nominal LHC parameters. Inserting these values into Eq. (13), we estimate an instability rise time of 50 ms for the horizontal and 400 ms for the vertical plane.

4 SIMULATION RESULTS FOR THE VLHC

Simulations of the electron-cloud instability in the VLHC were carried out with the same program as used for the LHC studies. We recall that in the simulation the photoelectrons are launched with an initial uniform distribution around the vacuum-chamber aperture, which is a good approximation, provided the photon reflectivity of the beam pipe is considerably larger than 50%, and that the number of photoelectrons is taken as approximately equal to the number of emitted photons, *i.e.*, that an effective photoemission yield (including conversion after reflection) close to unity is assumed. Since the VLHC chamber wall could be coated to reduce the photoemission, we have simulated how sensitive the instability rise time is to the number of primary photoelectrons. As for the LHC, we have also studied the dependence of the effective wakefield in the VLHC on the secondary-emission yield. This dependence could be more important than in the LHC case, since for aluminum or, more precisely, for an aluminum-oxide surface layer the secondary-emission yield is very high. Values of δ_{max} quoted in the literature vary between about 2.6 and 3.5. If necessary, the yield could be drastically reduced with a titanium nitride coating, as it is applied to the aluminum vacuum chamber of the PEP-II Low Energy Ring and considered for the LHC beam screen.

Since, as we shall see, at the VLHC most secondary electrons are generated by primary electrons which have

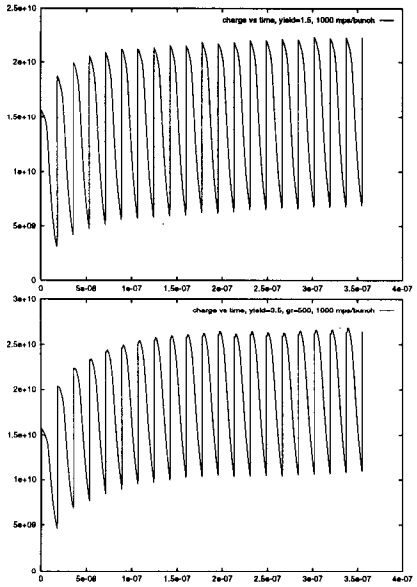

Figure 13: Charge of the electron cloud (in units of e) accumulated inside a VLHC bending magnet as a function of time (in s), for two different values of the maximum yield δ_{max}; top: $\delta_{max} = 1.5$; bottom: $\delta_{max} = 3.5$. The total time span corresponds to 21 bunch passages, which are reflected in the sawtooth-like evolution pattern. In this simulation, 1000 macroparticles per bunch were launched, and the grid size for the space-charge calculation was 500 points.

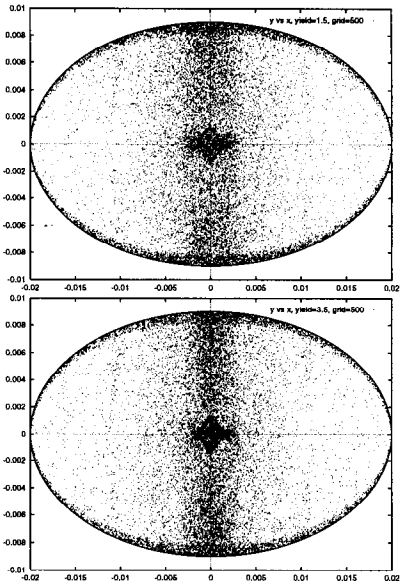

Figure 14: Transverse distribution of macroelectrons in a VLHC bending magnet after 20 bunches for a maximum secondary emission yield δ_{max} of 1.5 (top) and 3.5 (bottom). Horizontal and vertical dimensions are given in units of m.

come very close to the beam, particular care must be taken to model the motion of such electrons as accurately as possible. Inserting the VLHC parameters into Eq. (8), we find that the minimum number of tracking steps during a single bunch passage must be chosen larger than [28] $n_{\rm slice} \approx 100$. To restrict the computation time, we chose a smaller number of steps per bunch, $n_{\rm slice} \approx 30$. From the variation of the results over different random seeds, we estimate that the error thereby introduced is not larger than 10–20%.

Figure 13 shows simulation results of the electron-cloud build-up inside a VLHC bending magnet, for two different values of the secondary-emission yield. In both cases the charge density saturates after the passage of less than 10 bunches. For these parameters the neutralization density (at which the number of electrons in the beam pipe equals the time-averaged number of protons) amounts to a total electron charge of about 5×10^{11} e per bend, which is roughly a factor of 2 higher than the saturation values observed in Fig. 13.

In Fig. 14, the transverse macroparticle distribution after the passage of 20 bunches is depicted for two different values of the secondary-emission yield δ_{max}. For both cases, we notice a vertical stripe of increased electron density near the center of the beam pipe. From these two pictures, it is difficult to discern significant differences in the results for the two secondary-emission yields. The situation changes, when, instead of the macroelectron density, we look at their charge distribution. The projected horizontal and vertical charge distributions are shown in Fig. 15. For the higher secondary emission yield (bottom picture), a narrow stripe of increased electron density is visible around the center of the beam pipe, which we may attribute to the higher electron energies and the consequently greater secondary-emission yield in this region. If the maximum yield is lower, such as $\delta_{max} = 1.5$ (top picture), the secondary emission is less important, and the electron distribution, which is now dominated by the primary photoelectrons, becomes more uniform.

Table 3 lists the simulated effective bunch-to-bunch wake function $W_1(L_{sep})$ for the VLHC, under several different conditions. The table demonstrates that lowering the maximum secondary-emission yield δ_{max} from 3.5 to 1.5 does not significantly affect the vertical wakefield, while it leads to a sign reversal of the horizontal wakefield! The large sensitivity of the horizontal wake to the secondary emission yield appears to have the same origin as the difference in the two horizontal density projections of Fig. 15. A possible explanation is the following.

If a bunch is displaced horizontally, the electrons closer to the displaced bunch are more strongly accelerated by the beam field than the electrons on the other side of the vacuum chamber. For a large secondary emission yield, these higher-energetic electrons generate a lot of secondaries. When the following bunch passes by (which is assumed to be on the design orbit at the center of the beam pipe), it will be deflected by these secondary electrons in the same direction in which the previous bunch was dis-

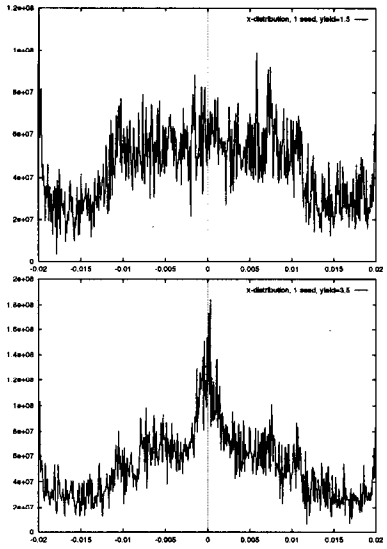

Figure 15: Projected horizontal electron charge density in a VLHC bending magnet after 20 bunches, as obtained for one random seed, and a yield of $\delta_{max} = 1.5$ (top) and $\delta_{max} = 3.5$ (bottom). The horizontal coordinate is given in units of meters; the vertical coordinate is the charge (in units of e) per bending magnet, per bin and per grid point. The total number of grid points is 500, and 1000 macroparticles per bunch (and per seed) were used.

placed. This means that the wakefield has a positive sign. On the other hand, when the secondary emission yield is low, the primary electrons closer to the displaced bunch because they acquire a larger speed have a higher probability to be lost before the next bunch arrives, but, for a reduced yield δ_{max}, they do not generate as many secondaries. The next bunch then interacts with an electron cloud whose centroid charge is on the side opposite from the displaced bunch. Therefore, in this case the effective wakefield is negative.

To demonstrate the correctness of this interpretation, Fig. 16 shows horizontal projections of the electron charge distribution just prior to the arrival of the 22nd bunch after the 21st bunch was displaced horizontally by 5 mm. Depicted are simulation results for three different values of the secondary emission yield. It is obvious that the charge centroid shifts from the left to the right, as the emission yield increases, which is consistent with the observed sign reversal of the horizontal wakefield.

Reducing the number of photoelectrons emitted per photon by a factor of 4 results in a 50% smaller vertical wakefield, while the horizontal wakefield remains essentially unchanged (in Table 3 this case is indicated by the comment '$\eta_{pe}^{eff} = 0.25$').

From Table 3, the integrated dipole wake functions $W_{1,x}(L_{sep})$ and $W_{1,y}(L_{sep})$ at a distance equal to the bunch spacing are about $8\text{–}9\times10^6$ m^{-2} and $9\text{–}(-15)\times10^6$ m^{-2}, respectively, for the nominal photoemission yield and a secondary-emission yield ranging from $\delta_{max} = 3.5$ to

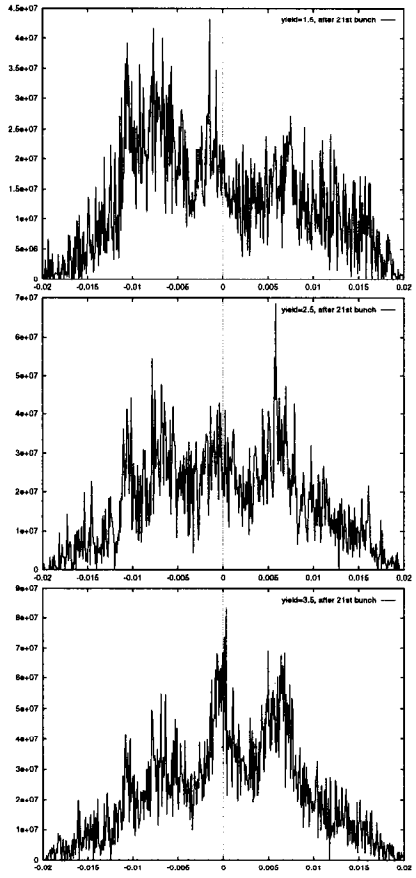

Figure 16: Projected horizontal electron charge density in a VLHC bending magnet just prior to the arrival of the 22nd bunch, when the 21st bunch was displaced by 5 mm. Shown are pictures for three different secondary emission yields: $\delta_{max} = 1.5$ (top), $\delta_{max} = 2.5$ (center), $\delta_{max} = 3.5$ (bottom). The horizontal coordinate is in units of meters; the vertical coordinate is the charge (in units of e) per bending magnet, per bin and per grid point. The total number of grid points is 500, and 1000 macroparticles per bunch (and per seed) were used.

δ_{max}	$W_{1,y}$ (10^6 m^{-2})	$W_{1,x}$ (10^6 m^{-2})	comment
3.5	9.4 ± 1.9	8.9 ± 2.2	—
2.5	8.8 ± 1.2	-2.2 ± 1.3	—
1.5	8.1 ± 0.9	-14.6 ± 1.8	—
2.5	4.5 ± 0.7	-2.9 ± 0.8	$\eta_{pe}^{eff} = 0.25$

Table 3: Effective bunch-to-bunch dipole wake function in the bending magnets of the VLHC, estimated by displacing the 20th bunch in the train and calculating the induced deflection of the following bunch. All simulations were performed with 1000 macroparticles per bunch and with a transverse drive-bunch displacement equal to 0.3 cm. The different rows refer to various secondary emission yields, macroparticle numbers, transverse offsets, charges per bunch, and effective photoemission yields. The comment $\eta_{pe}^{eff} = 0.25$ refers to a reduction of the photoemission probability by a factor of 4, compared with the nominal case.

$\delta_{max} = 1.5$. Assuming that the wakefield decays rapidly and only affects the next bunch, we can use Eq. (13) to estimate an instability rise time of about 3–4 s for both the horizontal and the vertical plane. The vertical instability rise time doubles, when the photoemission yield is reduced by a factor of 4, while the horizontal rise time is less sensitive to the photoemission, but depends much more strongly on the secondary emission yield.

5 CONCLUSIONS

We have simulated the build-up of an electron cloud that is generated by photoemission and secondary emission in the LHC and VLHC beam pipes. Based on the simulation results, the effect of the electron cloud on the beam stability was estimated.

Our preliminary conclusion is that, in the LHC, the electron cloud gives rise to a multi-bunch instability at top energy with an approximate rise time of the order of 50 ms in the horizontal and 400 ms in the vertical direction. The rise time is almost comparable to that of the resistive-wall instability at injection energy. The electron-cloud instability is driven primarily in the bending magnets, while the effective 'wakes' in the straight sections are 3–15 times smaller. For the parameters considered, the computed wakefield is not very sensitive to the secondary-emission yield δ_{max}, but it shows a strong dependence on the energy distribution of the secondary electrons.

In the VLHC, the rise time of the electron-cloud instability was estimated to be of the order of 3–4 s, and, in general, it appears to be of similar strength in the two transverse planes. This is different from the LHC case, which can be attributed to the different vacuum-chamber aspect ratio and the different beam current. In the VLHC, the effective vertical wakefield is fairly independent of the assumed secondary emission yield δ_{max}, whereas the horizontal wakefield reverses its sign at a yield value δ_{max} slightly above 2.5. This sign reversal is caused by a change of the relative importance of photoemission and secondary emission and by the accompanying change in the response of the electron cloud to horizontal bunch displacements.

The LHC (and VLHC) conditions do *not* seem to require a precise synchronism between electron motion and proton bunches, in order for the electron-cloud instability to become important. Since the simulation results show little change over a fairly wide range of parameters, they are probably not 'accidental'. That the electron-cloud instability has not been observed in other proton storage rings, such as HERA-p or the Tevatron, can be explained by the much lower critical energy (< 0.2 eV) in these machines: if the typical photon energy is much smaller than the work function of the beam-pipe material, the probability of photoemission is reduced by many orders of magnitude.

To safely damp the electron-cloud instability, in the LHC (VLHC) a bunch-by-bunch feedback system with a response time of about 20 ms (1 s) will be necessary. Even if it is damped by such a feedback system, the instability may still lead to an incoherent emittance growth. Also higher-order instability modes (e.g., quadrupole, sextupole mode...) could occur [34]. These modes may be excited by the beam-beam interaction [34] and are not easily damped by a feedback. As an alternative cure, the instability growth rate may be decreased by introducing additional gaps in the bunch train. In a gap of 2–3 bunch places almost all electrons will be lost. Our simulations suggest that such gaps must occur very frequently, i.e., about every 5–10 bunches.

All the results presented are preliminary. In the future, the simulations can be improved and extended in various regards, for instance, by

1. solving the Poisson equation with a 2-dim. FFT or by using a 2-dim. (3.-dim.) particle-in-cell code to more accurately represent the electron space-charge field,
2. including the effect of the magnetic field of the beam on the electron motion,
3. a fully relativistic treatment of the electron motion in all three directions,
4. using the real beam-screen dimensions instead of an elliptical approximation,
5. calculating the effective quadrupole wakefield, and
6. a careful revision of all the underlying assumptions.

The secondary emission yield of a copper (or aluminum) vacuum chamber can be reduced by coating with an appropriate material such as TiN or TiZr [6]. Measurements of secondary emission and photoemission on vacuum-chamber prototypes would be a useful input for future studies. In particular, the sensitivity of the secondary-emission yield to a strong magnetic field, its dependence on the incident angle and, for the LHC, the effect of physisorbed hydrogen molecules at the beam-screen surface should be investigated. One may also hope to reduce

the photoemission yield by special surface treatments, although the simulation results suggest that a moderate reduction of the photoemission yield is unlikely to significantly suppress the instability.

Finally, it should be mentioned that, in addition to causing a transverse beam instability, the large number of electrons bouncing in the beam pipe will raise the average vacuum pressure and, in case of the LHC, the heat load on the cryogenic system. These aspects will require more detailed simulation studies. Preliminary estimates suggest that the additional heat load due to the electron cloud could be substantial [35, 36, 37, 38].

6 ACKNOWLEDGEMENTS

I would like to thank Prof. S. Kurokawa, Dr. Y.H. Chin, Dr. Y. Funakoshi, Ms. Y. Hayashi and many more colleagues from KEK for the invitation to this workshop, the perfect organization, the warm hospitality, several stimulating discussions, and for financial support.

I am very grateful to Dr. F. Ruggiero from CERN for guidance, help, discussions during the course of this work and for a careful reading of an earlier manuscript. Many thanks also go to Dr. O. Brüning for discovering several errors in the original simulation program and for some very helpful suggestions. Dr. M. Furman, Dr. S. Heifets, Dr. T. Raubenheimer, Dr. O. Gröbner, Dr. C. Benvenuti, Dr. G. Lambertson, Dr. J. Seeman, Dr. M. Zisman, Dr. S. Mitsunobu, and Dr. W. Stoeffl deserve my thanks for many useful informations and various stimulating discussions.

The work reported here has been strongly inspired by similar simulation studies which Dr. M. Furman has recently performed for PEP-II, and by Dr. S. Heifets' analytical calculations. In addition, I am grateful to Dr. E. Malamud and Dr. J. Holt from Fermilab for suggesting the study of the electron-cloud instability in the VLHC.

Finally, I want to thank the AP group of the CERN SL division, in particular Dr. F. Ruggiero, Dr. J. Gareyte and Dr. J.-P. Koutchouk, for an invitation to CERN last February, for hospitality and support, and Dr. M. Böge and Dr. H. Grote for their help with the CERN computer system.

7 REFERENCES

[1] K. Ohmi, "Beam-Photoelectron Interactions in Positron Storage Rings", Phys. Rev. Lett., Vol. 75, No. 8 (1995).

[2] O. Gröbner, 10th Int. Conference on High Energy Accelerators, Protvino (1977).

[3] The Large Hadron Collider, Conceptual Design, CERN/AC/95-05 (1995); note that the dimensions of the beam screen have been slightly increased to the values quoted, since this report was written.

[4] E. Malamud, private communication (1997).

[5] O. Brüning and F. Ruggiero, private communication (1997).

[6] C. Benvenuti, private communication (1997).

[7] M. Izawa et al., "The Vertical Instability in a Positron Bunched Beam", Phys. Rev. Lett., Vol. 74 No. 8 (1995).

[8] S. Kurokawa, private communication (1997).

[9] M. Furman and G. Lambertson, talk for PEP-II Machine Advisory Committee and updates, January 1997 (1997).

[10] S.A. Heifets, "Transverse Instability Driven by Trapped Electrons", SLAC/AP-95-101 (1995).

[11] W. Stoeffl, private communication (1994).

[12] O. Gröbner, "Technological problems related to the cold vacuum system of the LHC", Vacuum, vol. 47, pp. 591–595 (1996).

[13] H.G. Hereward, CERN 71-15 (1971).

[14] E. Keil and B. Zotter, CERN-ISR-TH/71-58 (1971).

[15] F. Zimmermann, "A Simulation Study of Electron-Cloud Instability and Beam-Induced Multipacting in the LHC", CERN LHC Project Report 95 and SLAC-PUB-7425 (1997).

[16] A.V. Burov and N.S. Dikansky, "Electron-Cloud Instabilities", Novosibirsk, presented at this workshop, Tsukuba, (1997).

[17] F. Zimmermann, "Electron-Cloud Instability in the VLHC", SLAC/AAS-91 (1997).

[18] M. Sands, "The Physics of Electron Storage Rings", SLAC-121 (1970).

[19] J. Kouptsidis and G.A. Mathewson, DESY 76/49 (1976).

[20] World-wide web page 'http://www-cxro.lbl.gov/optical_constants/' published by the LBNL X-ray laboratory.

[21] M. Furman, private communication (1996).

[22] M. Zisman, private communication (1996).

[23] S. Heifets, private communication (1997).

[24] H. Bruining, "Physics and Applications of Secondary Electron Emission", Pergamon Press (1954).

[25] H. Seiler, "Secondary electron emission in the scanning electron microscope", J. Appl. Phys. 54 (11) (1983).

[26] M. Furman, private communication (1996).

[27] The importance of this effect, in particular for the PEP-II chamber, was mentioned by T. Raubenheimer (1997).

[28] J.S. Berg, "Energy Gain in an Electron Cloud During the Passage of a Bunch", CERN Project Note 97 (1997).

[29] F. Ruggiero, private suggestion (1997).

[30] T. Raubenheimer, private communication (1997).

[31] O. Brüning, private communication (1997).

[32] A. Chao, "Physics of Collective Beam Instabilities in High Energy Accelerators", Wiley, p. 208 (1995).

[33] S. Mitsunobu, private suggestion at this workshop (1997).

[34] J. Gareyte, private communication (1997).

[35] O. Gröbner, "Beam-Induced Multipacting", presented at PAC97 Vancouver (1997).

[36] M. Furman, private communication (1997).

[37] O. Brüning, private communication (1997).

[38] F. Ruggiero, private communication (1997).